The Atg8 Conjugation System Is Indispensable for Proper Development of Autophagic Isolation Membranes in Mice

Yu-shin Sou,*†‡ Satoshi Waguri,‡§ Jun-ichi Iwata,*†‡ Takashi Ueno,†∥
Tsutomu Fujimura,∥ Taichi Hara,¶ Naoki Sawada,§ Akane Yamada,§
Noboru Mizushima,¶# Yasuo Uchiyama,@ Eiki Kominami,† Keiji Tanaka,*
and Masaaki Komatsu*†**

*Laboratory of Frontier Science, Tokyo Metropolitan Institute of Medical Science, Bunkyo-ku, Tokyo 113-8613, Japan; †Department of Biochemistry, Juntendo University School of Medicine, Bunkyo-ku, Tokyo 113-8421, Japan; §Department of Anatomy and Histology, Fukushima Medical University School of Medicine, Fukushima 960-1295, Japan; ∥Division of Proteomics and Biomolecular Science, Juntendo University School of Medicine, Bunkyo-ku, Tokyo 113-8421, Japan; ¶Department of Physiology and Cell Biology, Tokyo Medical and Dental University Graduate School and Faculty of Medicine, Bunkyo-ku, Tokyo 113-8519, Japan; #SORST, Japan Science and Technology Corporation, Kawaguchi 332-0012, Japan; @Department of Anatomy, Juntendo University School of Medicine, Bunkyo-ku, Tokyo 113-8421, Japan; and **PRESTO, Japan Science and Technology Corporation, Kawaguchi 332-0012, Japan

Autophagy is an evolutionarily conserved bulk-protein degradation pathway in which isolation membranes engulf the cytoplasmic constituents, and the resulting autophagosomes transport them to lysosomes. Two ubiquitin-like conjugation systems, termed Atg12 and Atg8 systems, are essential for autophagosomal formation. In addition to the pathophysiological roles of autophagy in mammals, recent mouse genetic studies have shown that the Atg8 system is predominantly under the control of the Atg12 system. To clarify the roles of the Atg8 system in mammalian autophagosome formation, we generated mice deficient in *Atg3* gene encoding specific E2 enzyme for Atg8. *Atg3*-deficient mice were born but died within 1 d after birth. Conjugate formation of mammalian Atg8 homologues was completely defective in the mutant mice. Intriguingly, Atg12–Atg5 conjugation was markedly decreased in *Atg3*-deficient mice, and its dissociation from isolation membranes was significantly delayed. Furthermore, loss of *Atg3* was associated with defective process of autophagosome formation, including the elongation and complete closure of the isolation membranes, resulting in malformation of the autophagosomes. The results indicate the essential role of the Atg8 system in the proper development of autophagic isolation membranes in mice.

INTRODUCTION

Proteolysis in eukaryotic cells can be separated largely into two major pathways: one pathway mediated by the proteasome and the other pathway by the lysosome. The proteasome, in collaboration with the sophisticated ubiquitin system for selection of target proteins, plays crucial roles in rapid and aggressive degradation of not only a variety of short-lived regulatory proteins but also abnormal proteins

with aberrant structures that should be eliminated from the cells to maintain cellular viability (Goldberg, 2003). In contrast, the lysosome is an organelle that contains a diverse array of hydrolases, which is separated from the cytosol by a limiting membrane to prevent the random destruction of cellular components. In this lysosomal pathway, degradation of plasma membrane proteins and extracellular proteins is mediated by endocytosis, whereas degradation of cytoplasmic components is achieved through autophagy, a process divided into three classes of pathways; macroautophagy, microautophagy, and chaperone-mediated autophagy (Cuervo, 2004; Klionsky, 2005).

Macroautophagy (hereafter referred to as autophagy) is the main route for sequestration of bulky portions of the cytoplasm into the lysosome. The initial steps of autophagy are the formation and subsequent elongation of the isolation membrane. The isolation membrane then enwraps cytoplasmic constituents such as organelles until its edges fuse with each other to form a double-membrane structure called the autophagosome. Finally, the outer membrane of the autophagosome fuses with the lysosome/vacuole; thereby the sequestered cytoplasmic components together with the inner membrane of the autophagosomes are completely de-

graded by the lysosomal/vacuolar hydrolases (Mizushima *et al.*, 2002).

There is general agreement that the most important role of autophagy is the supply of amino acids under nutrient-poor conditions in yeast and neonate starvation period in mice (Tsukada and Ohsumi, 1993; Kuma *et al.*, 2004; Komatsu *et al.*, 2005). In addition, it is also noted that constitutive autophagy, which occurs even under nutrient-rich conditions, is indispensable for cell homeostasis. In fact, autophagy deficiency in the CNS and the liver leads to neurodegeneration and liver dysfunction, respectively (Komatsu *et al.*, 2005, 2006, 2007; Hara *et al.*, 2006). Moreover, autophagy plays a vital role in cellular remodeling during differentiation and development of multicellular organisms, such as fly, worm and slime mold (Levine and Klionsky, 2004) and cellular defense against invading streptococcus (Gutierrez *et al.*, 2004; Nakagawa *et al.*, 2004). Plants lacking autophagy show accelerated senescence (Hanaoka *et al.*, 2002).

In the last decade, a set of genes, essential for autophagosome formation, were specified in yeast (Tsukada and Ohsumi, 1993; Thumm *et al.*, 1994) and most of them are conserved in mammals. Among them, gene products involved in Atg (*autophagy*) conjugation systems were identified, in which the enzymatic reactions involved are, in principle, analogous to the ubiquitin conjugation system, including E1 (activating enzyme) and E2 (conjugating enzyme) (Ohsumi, 2001). Both ubiquitin-like modifiers, Atg12 and Atg8, are activated by a common E1-like enzyme, Atg7, and transferred to two different E2-like enzymes, Atg10 and Atg3, respectively (Mizushima *et al.*, 1998a,b; Shintani *et al.*, 1999; Tanida *et al.*, 1999, 2002; Ichimura *et al.*, 2000). Although Atg12 forms an isopeptide bond with Atg5, which is the only specific target reported so far, Atg8 forms an amide bond with phosphatidylethanolamine (PE) dependent on Atg12–Atg5 conjugation (Ichimura *et al.*, 2000; Mizushima *et al.*, 2001). The Atg12–Atg5 conjugate interacts with another ATG gene product Atg16, to ultimately form a tetrameric complex in yeast (Kuma *et al.*, 2002). Mammalian Atg16 counterpart Atg16L also orchestrates a high molecular complex with Atg12–Atg5 conjugate (Mizushima *et al.*, 2003). Although Atg12–Atg5 conjugation is indispensable for elongation of the isolation membrane, the PE-bound microtubule-associated protein 1 light chain 3/MAP1LC3 (LC3-II) (mammalian Atg8 homologue) is considered important for maturation of autophagosomes (Kabeya *et al.*, 2000; Mizushima *et al.*, 2001). Indeed, the Atg12–Atg5–Atg16L complex is localized on the isolation membranes during their elongation and disassociated from them before completion of autophagosomal formation (Mizushima *et al.*, 2003). In comparison, the LC3-II stays on the outer and inner membranes of the isolation membranes until completion of autophagosome formation. In the final stage, LC3-II on the inner membrane is degraded by fusion of autophagosomes to lysosomes, whereas LC3-II on the outer membrane is released from autophagosomes by a specific cysteine protease, Atg4 (Kirisako *et al.*, 2000; Tanida *et al.*, 2004). Importantly, the attachment of PE to LC3 is almost completely impaired in *Atg5*-knockout cells, indicating that these two LC3/Atg8 and Atg12 conjugation systems contribute to the formation of autophagosomes in a cooperative manner (Mizushima *et al.*, 2001). Moreover, it became clear that the Atg12–Atg5 conjugate functions as an E3-like enzyme for the Atg8 lipidation reaction (Hanada *et al.*, 2007; Fujita *et al.*, 2008).

In the present study, we analyzed the specific role(s) of LC3/Atg8 conjugation in mammals. To do this, we gener-

ated mice lacking Atg3, the specific E2-like enzyme for the Atg8 conjugation system, and we found that lack of Atg3 severely suppressed the formation of Atg12–Atg5 conjugate as well as completely impaired Atg8 conjugation. Surprisingly, loss of Atg3 also resulted in the accumulation of small autophagosome-like structures or disorganized isolation membranes, indicating that Atg8 conjugation plays a critical role in the proper development of isolation membranes. We also discuss the precise roles of the Atg8 conjugation system in the autophagic pathway, based on phenotypic analyses of *Atg3* null-mice.

MATERIALS AND METHODS

Generation of Atg3$^{-/-}$ Mice

A targeting vector for *Atg3* was designed to disrupt exon 10, which codes the active site cysteine, by neo-resistant gene cassette. The targeting vector was electroporated into mouse TT$_2$ embryonic stem (ES) cells, selected with G418 (200 μg/ml; Invitrogen, Carlsbad, CA), and then screened for homologous recombinants by Southern blot analyses. Southern blot analysis was performed by digestion of genomic DNA with PstI and hybridization with the *Atg3* probe. Genotyping of mice was performed by polymerase chain reaction (PCR) using the two primers sets: one set was Atg3-S1 (5′-TAGGAGCCATT-TGCCACCAATCGTA-3′) and Neopr2Rv (5′-GCACTTCGCCCAATAGCAGCCA GTCCCTTC-3′), and the other set was Atg3-671-691 (5′-GGCAGCCTTTAACAGT-TGAGC-3′) and Atg3S-1. To generate *Atg3*$^{-/-}$ mice with green fluorescent protein (GFP)-LC3, we crossed *Atg3*$^{+/-}$ mice with GFP-LC3 transgenic mice (Mizushima *et al.*, 2004). Mice were housed in specific-pathogen free facilities, and the experimental protocol was approved by the Ethics Review Committee for Animal Experimentation of Tokyo Metropolitan Institute of Medical Science.

Generation of Mouse Embryonic Fibroblasts (MEFs)

MEFs were prepared as described previously (Komatsu *et al.*, 2005). Immortalized wild-type and *Atg3*-deficient MEFs were established by infecting MEFs with a recombinant retrovirus carrying a temperature-sensitive simian virus 40 large T antigen (Lee *et al.*, 1995). GFP-tagged Atg5 and FLAG-tagged Atg12 were subcloned into retrovirus vector pMXs-puro (Kitamura *et al.*, 2003). As described recently (Ichimura *et al.*, 2008), each GFPAtg5 and FLAGAtg12 vector was introduced into MEFs. To prepare Atg3 and Atg3C264S adenoviruses, we used the Adenovirus Expression Vector kit (Takara Bio, Otsu, Shiga, Japan). To express exogenous Atg3 and Atg3C264S proteins, the immortalized wild-type and *Atg3*-deficient MEFs were plated on six-well dishes in 2 ml of growth medium at 24 h before infection. The medium was replaced with fresh medium containing Atg3 or Atg3C264S adenovirus. The cells were lysed 48 h later, and then the lysates were analyzed by immunoblotting.

Immunological Analysis

Lysates of MEFs were immunoblotted as described previously (Komatsu *et al.*, 2005). The antibodies for Atg3, Atg7, Atg10, LC3, GABA(A) receptor-associated protein (GABARAP), and Golgi-associated ATPase enhancer of 16 kDa (GATE)-16 were described previously (Tanida *et al.*, 2002; Nemoto *et al.*, 2003; Komatsu *et al.*, 2005). The antibody for Atg16L was described previously (Mizushima *et al.*, 2003). The antibody against Atg12 was raised in rabbits using the recombinant protein as antigens. The antibody for actin (MAB1501R) was purchased from Millipore Bioscience Research Reagents (Temecula, CA) and that for Atg5 from Sigma (St. Louis, MO). For LC3 and Atg16L staining, MEFs were fixed and stained with anti-LC3 and anti-Atg16L antibodies, respectively, as described previously (Komatsu *et al.*, 2005). Fluorescence images were obtained using a fluorescence microscope (model BZ-9000; Keyence, Osaka, Japan). Atg16L-positive dots per each treated cell (n = 20) were counted using software Dynamic cell count BZ-HIC (Keyence).

Time-Lapse Imaging Analysis

Each genotype of MEF expressing GFPAtg5 was cultured in Hanks' solution for 1 h, and green fluorescent protein (GFP) images were taken every 30 s by using a fluorescence microscope (model BZ-9000; Keyence). Time-lapse recordings proceeded for 30 min at 37°C with a culture dish system (Keyence) for temperature and CO$_2$ control.

Pulse-Chase Experiments

Cells were incubated with cysteine- and methionine-free medium for 1 h, metabolically labeled with [^{35}S]cysteine and methionine for 2 or 24 h, and then washed and chased for the indicated time. The cell lysates were immunoprecipitated with M2 agarose (Sigma) or GFP agarose (Medical & Biological

Laboratories, Nagoya, Japan), fractionated by SDS-polyacrylamide gel electrophoresis (PAGE), and visualized by autoradiography.

Histological Examination

Methods for tissue fixation and subsequent procedures, including hematoxylin and eosin staining, immunofluorescence, conventional electron microscopy, and immunoelectron microscopy were described previously (Komatsu *et al.*, 2005, 2006). For pre-embedding immunoelectron microscopy, MEFs were fixed with 4% paraformaldehyde-4% sucrose in phosphate buffer (PB; pH 7.2) followed by permeabilization with 0.25% saponin/0.1 M PB. They were immunolabeled with anti-GFP or anti-Atg16L antibody and then with nanogold-conjugated anti-rabbit Fab' (Nanoprobes, Yaphank NY). After silver enhancement with HQsilver (Nanoprobes), they were embedded in Epon 812 and sectioned for electron microscopic observation. The number of each organelle was counted and expressed as the number per cell section or per 100 μm^2 of cytoplasmic area. The areas of the cytoplasm and autophagosomes were measured using MetaMorph image processing software (Molecular Devices, Sunnyvale, CA). Antibodies used for immunofluorescence and immunoelectron microscopy were as follow: rabbit polyclonal antibodies against Atg16L (Mizushima *et al.*, 2003) and GFP (Abcam, Cambridge, MA).

Other Procedures

RNA samples were extracted from each genotyping MEFs by using TRIzol reagent (Invitrogen). For RNA blot, 10 μg of RNA per samples was loaded. Blots were probed with Atg3- and actin-cDNA as control. Cell starvation was conducted by incubating the cells in Hanks' balanced solution with 10 mM HEPES, pH 7.5, following three separate washes. Caesarean delivery, mea-
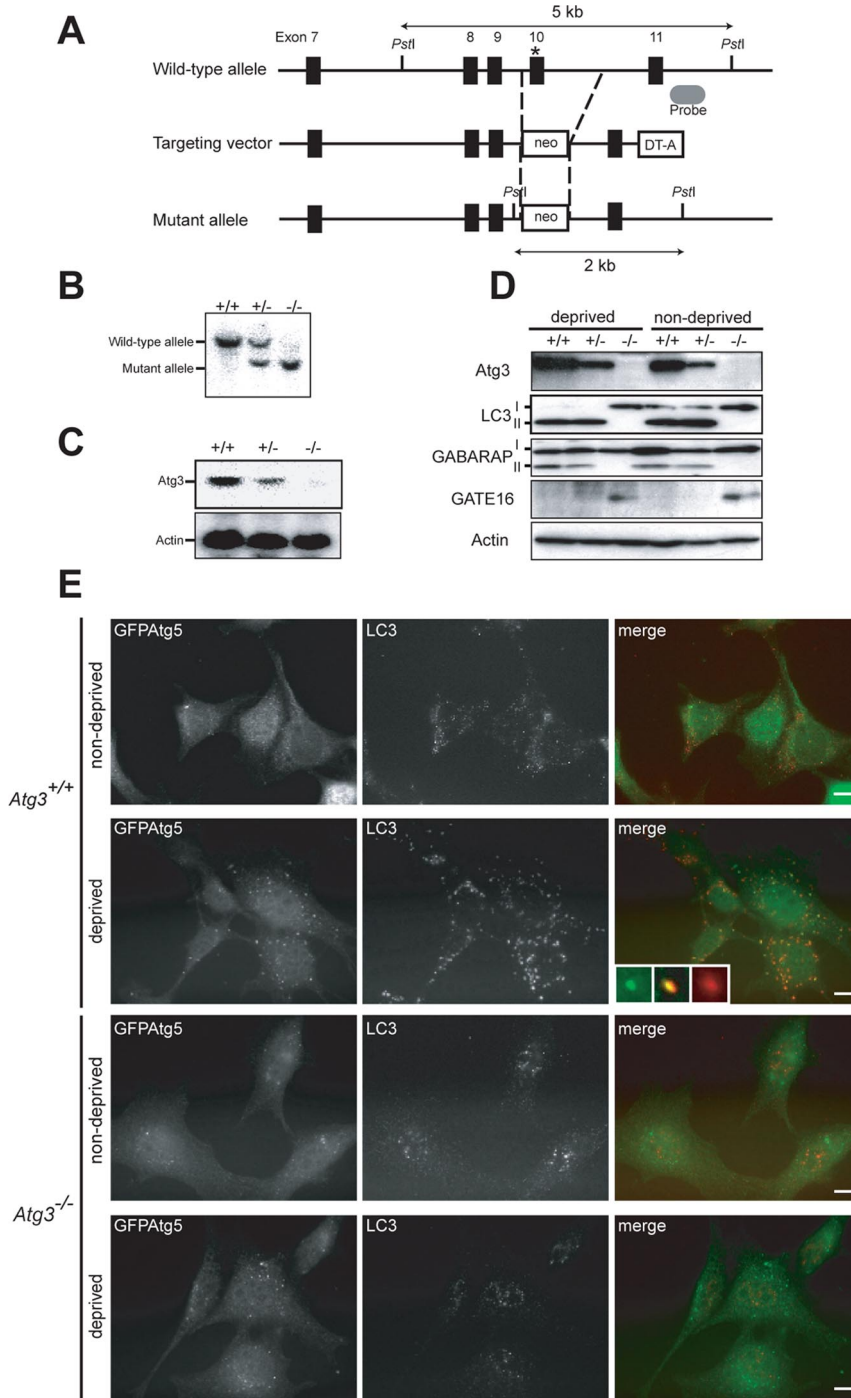

Figure 1. Generation of *Atg3*-knockout mice. (A) Schematic representation of the targeting vector and the targeted allele of *Atg3* gene. The coding exons numbered in accordance with the initiation site as exon 1 are depicted by black boxes. The probe for Southern blot analysis is shown as gray ellipse. The asterisk denotes the essential cysteine residue on exon 10. PstI, PstI sites; neo, neomycin-resistant gene cassette; DT-A, diphtheria toxin gene. (B) Southern blot analysis of genomic DNAs extracted from mice tails. Wild-type and mutant alleles are detected as 5- and 2-kb bands, respectively. (C) Expression of Atg3 transcript. Total RNAs were extracted from each genotyping MEFs. Atg3 transcript was detected by Northern blot with mouse Atg3 cDNA. Actin cDNA was used as an internal control. (D) Immunoblot of Atg3 and Atg8 homologues in MEFs. Primary MEFs of the indicated genotypes were isolated and cultured under nutrient-rich (nondeprived) and nutrient-poor (deprived) conditions. The lysates were immunoblotted with anti-Atg3, anti-LC3, anti-GABARAP, anti-GATE-16, and anti-actin antibodies. Data shown are representative of three separate experiments. (E) Immunofluorescence analysis of MEFs using anti-LC3antibody. Each genotype immortalized MEFs with introduced GFP-tagged Atg5 were cultured in DMEM with fetal calf serum (nondeprived) or Hanks' solution (deprived). The cells were fixed and then immunostained with anti-LC3. Insets show a GFPAtg5-single- (left inset), an LC3-single- (right inset), and a double-positive (middle inset) structure, respectively. Bars; 10 μm.

surement of amino acids, and assay of long-lived protein degradation were performed as reported previously (Komatsu *et al.*, 2005).

RESULTS

Generation of Atg3-Knockout Mice

To investigate the physiological roles of the Atg8 system in vivo, we generated mice deficient in Atg3, a specific E2-like enzyme for Atg8. Mouse *Atg3* gene is encoded by 12 exons that span 29.71 kb of genomic DNA. The active site cysteine residue, essential for conjugation of the substrates, is encoded by exon 10, and the targeting vector was designed to disrupt this exon by neo-resistant gene cassette (Figure 1A). Mice heterozygotes for the *Atg3* allele (referred to *Atg3$^{+/-}$* mice) were born healthy and fertile without any noticeable pathological phenotypes for 1 y. Figure 1B shows Southern blots of mice with the indicated genotypes. Neither Atg3 mRNA nor protein was detected in *Atg3$^{-/-}$* mice (Figure 1, C and D).

Shutdown of Atg8 System in Atg3-deficient Mice

We tested the loss of Atg3 activity by measuring the conversion of LC3 to its PE-conjugated form. To do this, we isolated MEFs from each genotype, followed by culture under nutrient-rich or starvation conditions and lysis. The lysates were subjected to SDS-PAGE followed by immuno-

blot analyses with anti-LC3 antibody. Mammalian Atg8p homologue LC3 exists in two forms in cells, LC3-I and LC3-II. LC3-I is a cytosolic form and LC3-II is a PE-conjugated form, which localizes in autophagosomes (Kabeya *et al.*, 2000). In *Atg3$^{+/+}$* and *Atg3$^{+/-}$* MEFs, both forms were detected under nutrient-rich condition, whereas only the LC3-II form was detected under starvation condition (Figure 1D), suggesting conversion of LC3-I in response to starvation. In contrast, only the LC3-I form was recognized in *Atg3$^{-/-}$* MEFs, regardless of the nutrient conditions. We also examined other Atg8 homologues, GABARAP and GATE-16 (Figure 1D). It is generally considered that they are also activated by Atg7, transferred to Atg3, and finally conjugated with PE for localization to autophagosomes (Tanida *et al.*, 2001, 2002; Kabeya *et al.*, 2004; Sou *et al.*, 2006). Whereas GABARAP-I (free form) was converted to GABARAP-II (PE-conjugated form) in wild-type and heterozygous MEFs and the level of conversion was not affected by starvation, its conversion was completely blocked in *Atg3$^{-/-}$* MEFs. Although GATE-16 was hardly detected in wild-type and heterozygous MEFs under both conditions, the band corresponding to GATE-16-I (free form) was clearly detected in *Atg3$^{-/-}$* MEFs (Supplemental Figure S1). Immunofluorescence analyses with anti-LC3 antibody revealed that starvation induced the appearance of LC3-positive dots in the
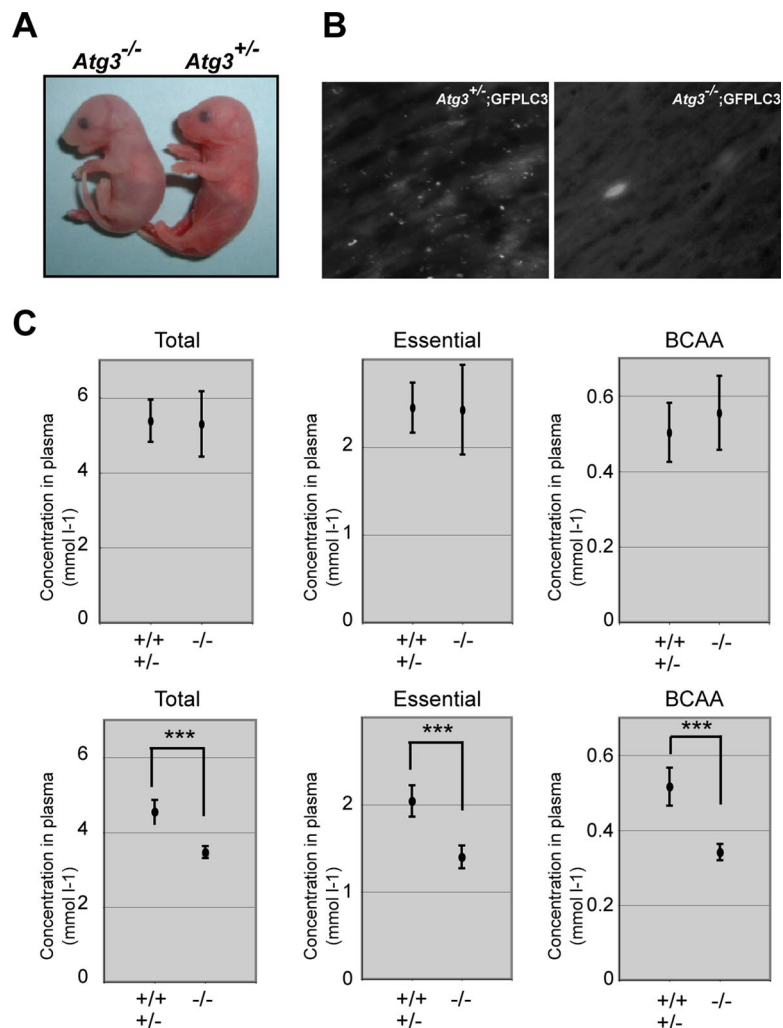

Figure 2. Phenotypes of *Atg3*-deficient mice. (A) Morphology of *Atg3$^{+/-}$* and *Atg3$^{-/-}$* mice. (B) Deficiency of LC3-positive dots in *Atg3$^{-/-}$* heart. *Atg3$^{+/-}$* and *Atg3$^{-/-}$* mice expressing GFP-LC3 were delivered by Cesarean section and analyzed by florescence microscopy. Representative results obtained from each neonatal heart at 3 h after Cesarean delivery. Bar; 50 μm. (C) The concentrations of total amino acids, essential amino acids, and BCAA in sera of mice of the indicated genotypes. *Atg3$^{+/+}$*, *Atg3$^{+/-}$* (n = 5) and *Atg3$^{-/-}$* mice (n = 4) were dissected immediately (top) or at 10 h (bottom) after delivery and the plasma concentrations of amino acids were measured. Data are mean ± SD. ***p < 0.001 by Student's *t* test.
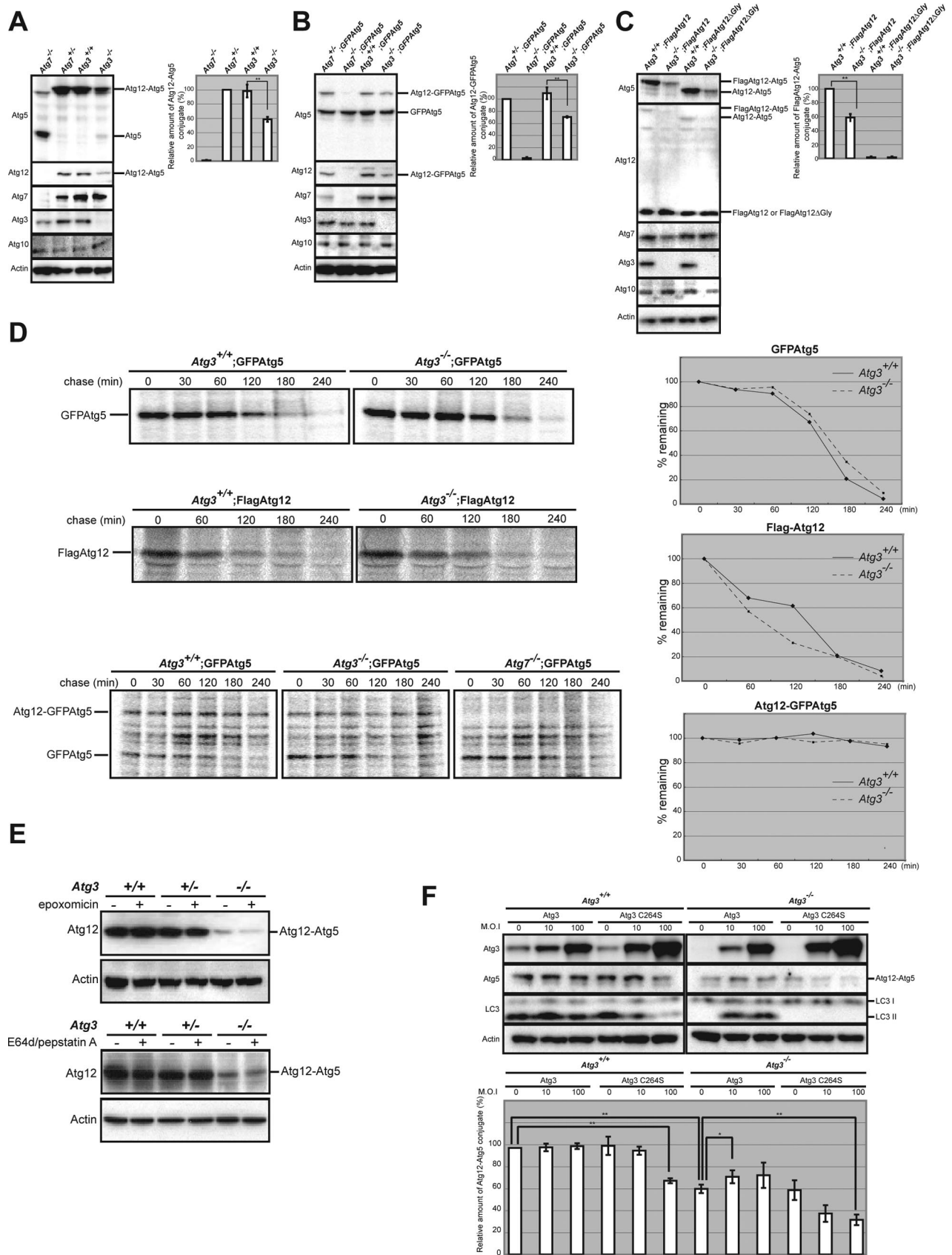
Figure 3. Formation of Atg12–Atg5 conjugates is partially inhibited by *Atg3* deficiency. (A) Immunoblot analyses of the Atg12–Atg5 conjugate. Immortalized MEFs of the indicated genotype were lysed, and the lysates were subjected to SDS-PAGE and analyzed by immunoblotting with the indicated antibodies. As a negative control for detection of Atg12–Atg5 conjugate, we used the lysate of

$Atg3^{+/+}$ but not in the $Atg3^{-/-}$ MEFs. In contrast, Atg5-positive dots were apparently induced in wild-type MEFs (Figure 1E), but no clear increase in $Atg3^{-/-}$ MEFs was evident because many of those were already formed even in nutrient-rich conditions (see Figure 4). Notably, in contrast with small dots containing only GFPAtg5 (left inset), the large structures (right inset) were almost singly positive for LC3, and the rest were positive for both proteins that were considered to be intermediate structures (middle inset). Together, these results suggest impairment of the Atg8 system in Atg3-knockout mice.

Phenotypes of Atg3-Knockout Mice

Although $Atg3^{-/-}$ mice were born at Mendelian frequency (+/+; +/−; −/− = 25; 38; 23), their body weight (0.99 ± 0.12 g; n = 8) was lower than that of wild-type and heterozygous mice (1.19 ± 0.105 g; n = 25; p < 0.002) (Figure 2A), and they died within 1 d after birth (n = 11), similar to Atg5 and Atg7 null-mice (Kuma et al., 2004; Komatsu et al., 2005). Autophagy is induced in newborn when the nutrients supply through the placenta terminates after birth (Kuma et al., 2004). To confirm this phenomenon, we crossed Atg3 with GFPLC3 transgenic mice (Mizushima et al., 2004) to generate $Atg3^{+/-}$ and $Atg3^{-/-}$ mice harboring GFP-LC3. Fasting for 3 h resulted in appearance of LC3-positive dots in $Atg3^{+/-}$;GFPLC3 but not $Atg3^{-/-}$;GFPLC3 hearts (Figure 2B). Lower production of amino acids correlates with the cause of death in autophagy-deficient mice (Kuma et al.,

2004; Komatsu et al., 2005). Therefore, we next measured the survival time of $Atg3^{-/-}$ neonates under starvation condition and measured serum amino acids concentrations after Caesarean delivery. $Atg3^{-/-}$ mice died at 13.2 ± 3.5 h after Caesarean delivery, although wild-type and heterozygous mice were alive at that time. The concentrations of total, essential and branched chain amino acids (BCAAs) in sera of $Atg3^{-/-}$ mice were almost comparable with those of wild-type mice at 0 h after Caesarean delivery but those of $Atg3^{-/-}$ were significantly lower at 10 h after Caesarean delivery compared with wild-type mice (Figure 2C). These results suggest that Atg3, similar to Atg5 and Atg7 (Kuma et al., 2004; Komatsu et al., 2005), is essential for the supply of amino acids into the blood circulation and survival of newborn mice under starvation condition.

Atg3 Deficiency Causes Reduced Formation of Atg12–Atg5 Conjugation

Atg5 deficiency leads to a significant reduction in LC3 conjugation to PE in yeast and mice as reported previously (Mizushima et al., 2001; Suzuki et al., 2001; Hosokawa et al., 2007), which could be explained by the E3-like activity of Atg12–Atg5 conjugate in Atg8-PE conjugation (Hanada et al., 2007; Fujita et al., 2008). Conversely, overproduction of Atg3 in human embryonic kidney 293 cells facilitates the formation of the Atg12–Atg5 conjugate (Tanida et al., 2002). These results suggest cooperation of the two conjugation systems during autophagosome formation. However, it is still puzzling how the Atg8/LC3 system affects the activity of the Atg12 system. To solve this puzzle, we conducted additional experiments in which each wild-type and Atg3-knockout MEFs were lysed and subjected to immunoblot analyses with anti-Atg12 and anti-Atg5 antibodies. Intriguingly, the amount of Atg12–Atg5 conjugate was markedly reduced in Atg3-deficient MEFs, whereas the amount of free Atg5 in the cells increased significantly (Figure 3A and Supplemental Figure S2). Even upon overexpression of either FLAG-tagged Atg12 or GFP-tagged Atg5, the efficiency of Atg12–Atg5 conjugation formation was still low in Atg3-deficient MEFs (Figure 3, B and C), suggesting the involvement of Atg3 in the conjugation reaction rather than the instability of individual components involved in the Atg12 system. In fact, the half-life of each of FLAGAtg12 and GFPAtg5 introduced into Atg3-deficient MEFs was comparable with that of wild-type MEFs (Figure 3D, top and middle). Importantly, once Atg12-GFPAtg5 conjugate was formed in Atg3-deficient cells, the conjugate was stable, similar to that in wild-type MEFs (Figure 3D, bottom). Furthermore, the amount of Atg12–Atg5 conjugates in Atg3-deficient MEFs did not change under treatment with epoxomicin, a proteasomal inhibitor (Figure 3E, top). We also confirmed that they did not change by treatment with E64d and pepstatin A, lysosomal inhibitors (Figure 3E, bottom). These results suggest inhibition of the Atg12–Atg5 conjugation reaction in Atg3-deficient MEFs.

Next, to determine whether the loss of E2 activity of Atg3 is involved in the reduced Atg12–Atg5 conjugate in Atg3-deficient MEFs, we used the mutant Atg3C264S. Atg3C264S has a mutation at the active site cysteine; thus, it is unable to form Atg8/LC3-PE conjugate. When Atg3 or Atg3C264S was expressed exogenously into Atg3-deficient MEFs by using adenovirus system, they were detected in sufficient amounts in both MEF genotypes (Figure 3F). Predictably, LC3 lipidation was complemented by exogenous expression of Atg3 but not Atg3C264S mutant (Figure 3F). Similarly, expression of Atg3, but not Atg3C264S mutant, recovered

Figure 3 (cont). Atg7-deficient MEFs. Note the low production of the Atg12–Atg5 conjugate in Atg3-deficient cells. (B) Each genotype immortalized MEFs with introduced GFP-tagged Atg5 were lysed, and then the lysates were subjected to SDS-PAGE followed by immunoblotting with the indicated antibodies. As a negative control for detection of Atg12–GFPAtg5 conjugate, we used the lysate of GFPAtg5-introduced Atg7-deficient MEFs. (C) Immortalized wild-type and Atg3-deficient MEFs-introduced FLAG-tagged Atg12 or Atg12ΔGly were lysed, and then the lysates were subjected to SDS-PAGE followed by immunoblotting with the indicated antibodies. As a negative control for detection of FLAGAtg12-Atg5 conjugate, we used the lysate of FLAGAtg12ΔGly-expressing MEFs. Graphs shown in A–C indicate the ratios of Atg12–Atg5, Atg12–GFPAtg5, and FLAGAtg12–Atg5 relative to actin, respectively. Data are mean ± SD of triplicate experiments. **p < 0.01 by Student's t test. (D) Half-lives of GFPAtg5, FLAGAtg12, and GFPAtg5-Atg12 conjugation in Atg3-deficient MEFs. Each immortalized wild-type and Atg3-deficient MEFs harboring GFPAtg5 or FLAGAtg12 were labeled with [^{35}S]cysteine and methionine for 2 h and chased for the indicated time. For labeling of GFPAtg5-12 conjugate, the cells were labeled with [^{35}S]cysteine and methionine for 24 h. Subsequently, each lysate was immunoprecipitated with anti-GFP and FLAG antibodies and then subjected to SDS-PAGE and visualized by autoradiography. As a negative control for detection of Atg12–GFPAtg5 conjugate, we used the lysate of GFPAtg5-introduced Atg7-deficient MEFs. The decay curves of GFPAtg5 (top, right), FLAGAtg12 (middle, right) and Atg12-GFPAtg5 (bottom, right) were generated from quantification of the band shown in the left panels. (E) The MEFs of the indicated genotypes were cultured in the presence or absence of a proteasome inhibitor (epoxomicin) for 16 h (top) or lysosomal inhibitors (E64d and pepstatin A: E/P) for 24 h (bottom). The cell lysates were subjected to SDS-PAGE and analyzed by immunoblotting with anti-Atg12 and anti-actin antibodies. (F) Wild-type and Atg3-deficient immortalized MEFs were infected with Atg3 and Atg3C264S at 10, or 100 multiplicity of infection (M.O.I.). After 48-h infection, the cell lysates were subjected to SDS-PAGE and analyzed by immunoblotting with the indicated antibodies. Bottom graph shows the ratios of Atg12–Atg5 relative to actin, respectively. Data are mean ± SD. **p < 0.01 by Student's t test. Data are representative of three separate experiments.
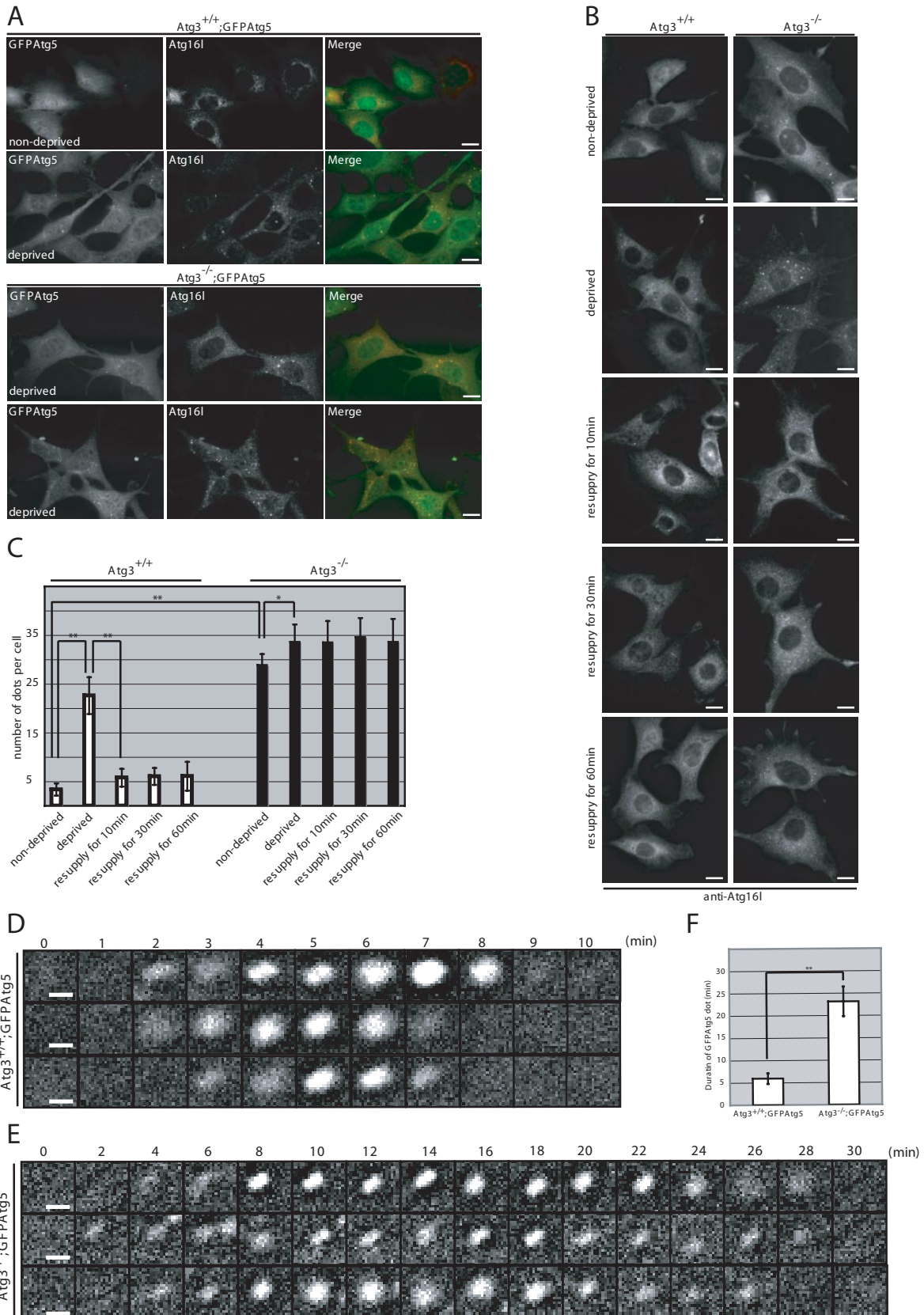
Figure 4. Accumulation of Atg16L-positive structures in *Atg3*-deficient MEFs. (A) Immunofluorescence analysis of Atg16L in GFPAtg5-introduced immortalized MEFs. Each genotype MEFs were cultured in nutrient-rich (nondeprived) or Hanks' solution (deprived). The cells were fixed and then immunostained with anti-Atg16L. Bars; 10 μm. (B) Immunofluorescence analysis of Atg16L in MEFs. MEFs isolated from *Atg3*^{+/+} and *Atg3*^{−/−} were cultured in nutrient-rich (nondeprived) or Hanks' solution (deprived). After deprivation of nutrients, the cells

partial defect in the Atg12–Atg5 conjugate in *Atg3*-deficient cells (Figure 3F). Moreover, expression of Atg3C264S into wild-type MEFs led to not only partial inhibition of LC3-PE but also suppression of the Atg12–Atg5 conjugate formation (Figure 3F). These results suggest that the Atg8/LC3 system participates in the reaction of Atg12–Atg5 conjugation through the E2 activity of Atg3.

Accumulation of Atg16L-positive Structures in Atg3-deficient MEFs

Next, we examined the localization of Atg16L and Atg5 in *Atg3*-deficient MEFs stably expressing GFPAtg5. It has been shown that Atg16L is localized in isolation membranes in Atg5-dependent manner and disassociated from the membrane before completion of autophagosome formation (Mizushima *et al.*, 2003). We also observed the induction of dot structures that were double positive for GFPAtg5 and Atg16L after nutrient deprivation in wild-type MEFs (Figure 4A). Although the Atg16L/GFPAtg5-positive dots were only rarely detected in wild-type MEFs in nutrient-rich conditions, these dots were distinctly observed in *Atg3*-deficient MEFs (Figure 4A). Moreover, their number was slightly but significantly increased upon nutrient deprivation (Figure 4, A and C), suggesting that the formation of isolation membranes is induced in response to starvation even in mutant cells. Wortmannin, an inhibitor of phosphatidylinositol 3-kinases, which are known to inhibit autophagy, suppressed the appearance of the GFPAtg5/Atg16L-positive dots during nutrient deprivation in both wild-type and mutant MEFs (Supplemental Figure S3). These results suggest that the appearance of GFPAtg5/Atg16L-positive dots in *Atg3*−/− MEFs is due to a standard autophagy mechanism requiring functional phosphatidylinositol 3-kinases. A similar Atg16L-staining pattern was also observed in *Atg3*-knockout MEFs without exogenous GFPAtg5, where almost all Atg5 existed as Atg12–Atg5 conjugates (Figures 3A and 4B), implying colocalization of Atg12–Atg5 conjugate and Atg16L in *Atg3*-deficient MEFs.

If elongation of isolation membrane and/or completion of autophagosome formation were impaired in *Atg3*-deficient cells, starvation-induced Atg16L-positive structures in mutant cells should remain even after the resupply of nutrients. As expected, although the starvation-induced Atg16L-positive structures disappeared within 10 min upon resupply of nutrients in wild-type MEFs, Atg16L-positive dots in mutant MEFs remained for 60 min after the resupply of nutrients (Figure 4, B and C). To directly determine the life span of these isolation membranes in *Atg3*-deficient MEFs, we carried out time-lapse video microscopic analysis. Consistent with the previous report (Mizushima *et al.*, 2001), upon nutrient deprivation, the GFPAtg5 dots occurred at random in the cytosol of wild-type MEFs, dwelled, and disappeared within ~5 min (Figure 4D and Supplemental Video 1). In contrast, although new GFPAtg5-dots in addition to the preexisting dots occurred in response to nutrient deprivation in the cytosol of mutant MEFs, the disappearance was significantly delayed; and in most cases, their presence was noted over >20 min (Figure 4E and Supplemental Video 2). Moreover, the numbers of de novo GFPAtg5-dots in wild-type and mutant MEFs under 10-min starvation conditions were 12.4 ± 2.2 and 8.7 ± 2.1, respectively (n = 5, p < 0.05). These results suggest impaired dissociation of the Atg12-Atg5-Atg16L complex from the isolation membranes in *Atg3*-deficient mice.

Appearance of Small Autophagosome-like Structures but Not Autolysosomes in Atg3-deficient Cells

Surprisingly, electron microscopic analyses revealed the presence of some autophagosome-like structures in *Atg3*-deficient MEFs cultured in normal media (Figure 5A), and their number was higher than in wild-type MEFs (Figure 5B). Nutrient deprivation induced a marked increase in the autophagosome-like structures even in *Atg3*-deficient MEFs (Figure 5, A and B), although the rate of increase was lower than that in wild-type MEFs (Figure 5B; see *Discussion*). However, quantitative analysis showed that the average size of the structures (represented as the encircled area) was smaller than that in wild-type MEFs cultured under nutrient-poor conditions (Figure 5C). The induction of autophagosome-like structures in mutant MEFs was suppressed by pretreatment with wortmannin (Supplemental Figure S4), suggesting that similar to the GFPAtg5/Atg16L-positive dots, these autophagosome-like structures are also derived from autophagic mechanisms involving the function of phosphatidylinositol 3-kinases.

To examine the fine structure of Atg5/Atg16L-positive dots, we carried out immunoelectron microscopic analysis in wild-type and *Atg3*-deficient MEFs expressing GFPAtg5. Two hours after starvation, silver-enhanced gold particles, representing GFPAtg5 or Atg16L, accumulated extensively on the small crescent-shaped membrane compartments in both wild-type and mutant MEFs (Figure 5D, b, c, e, and f), which are reported to represent the early developmental structures of the isolation membrane (Mizushima *et al.*, 2001; Mizushima *et al.*, 2003). Meanwhile, GFPAtg5 or Atg16L signal was hardly detected on the autophagosomal and autolysosomal membranes (Figure 5D, a and c). They were occasionally localized on the cup-shaped isolation membranes (Figure 5D, a and c) but with less intense signal compared with those on the crescent-shaped isolation membranes in both wild-type and mutant MEFs. It is of note that the atypical autophagosome-like structures described below (see Figure 7) in mutant MEFs also contained the signal for Atg16L (Figure 5Dh) and such Atg16L-positive structures were hardly observed in wild-type MEFs. These results indicate that most of the accumulated Atg5/Atg16L-positive structures observed by epifluorescent microscopy in the *Atg3*-deficient MEFs represent immature isolation membranes rather than autophagosome-like structures detected by electron microscopy.

Failure of Autolysosome Formation in Atg3-deficient MEFs

We also noticed that *Atg3*-deficient cells hardly contained autolysosomal structures, which contain a high electron-dense material with a hollow beneath the limiting membrane, which were otherwise usually detected in wild-type MEFs (Figure 5, A and B). To investigate whether this represents impaired autolysosome formation in *Atg3* deficiency, we examined protein degradation in *Atg3*-deficient cells un-

Figure 4 (cont). were resupplied with nutrients for 10, 30, or 60 min. The cells were fixed and then immunostained with anti-Atg16L. Bars; 10 μm. (C) The number of Atg16L-positive dots in MEF (n = 20) was determined in each genotype. Data are mean ± SD. *p < 0.05 and **p < 0.01 by Student's *t* test. (D and E) Time-lapse observation of starvation-induced GFPAtg5 dots. Wild-type (D) and *Atg3*-deficient (E) MEFs harboring GFPAtg5 were cultured in Hanks' solution for 1 h and directly observed by time-lapse video microscopy. Bars, 1 μm. (F) Duration of existence of GFPAtg5 dots in wild-type and *Atg3*-deficient MEFs. The time of sustained presence of GFPAtg5 dots in wild-type (n = 9) and mutant (n = 10) was measured. Data are mean ± SD. **p < 0.01 by Student's *t* test.
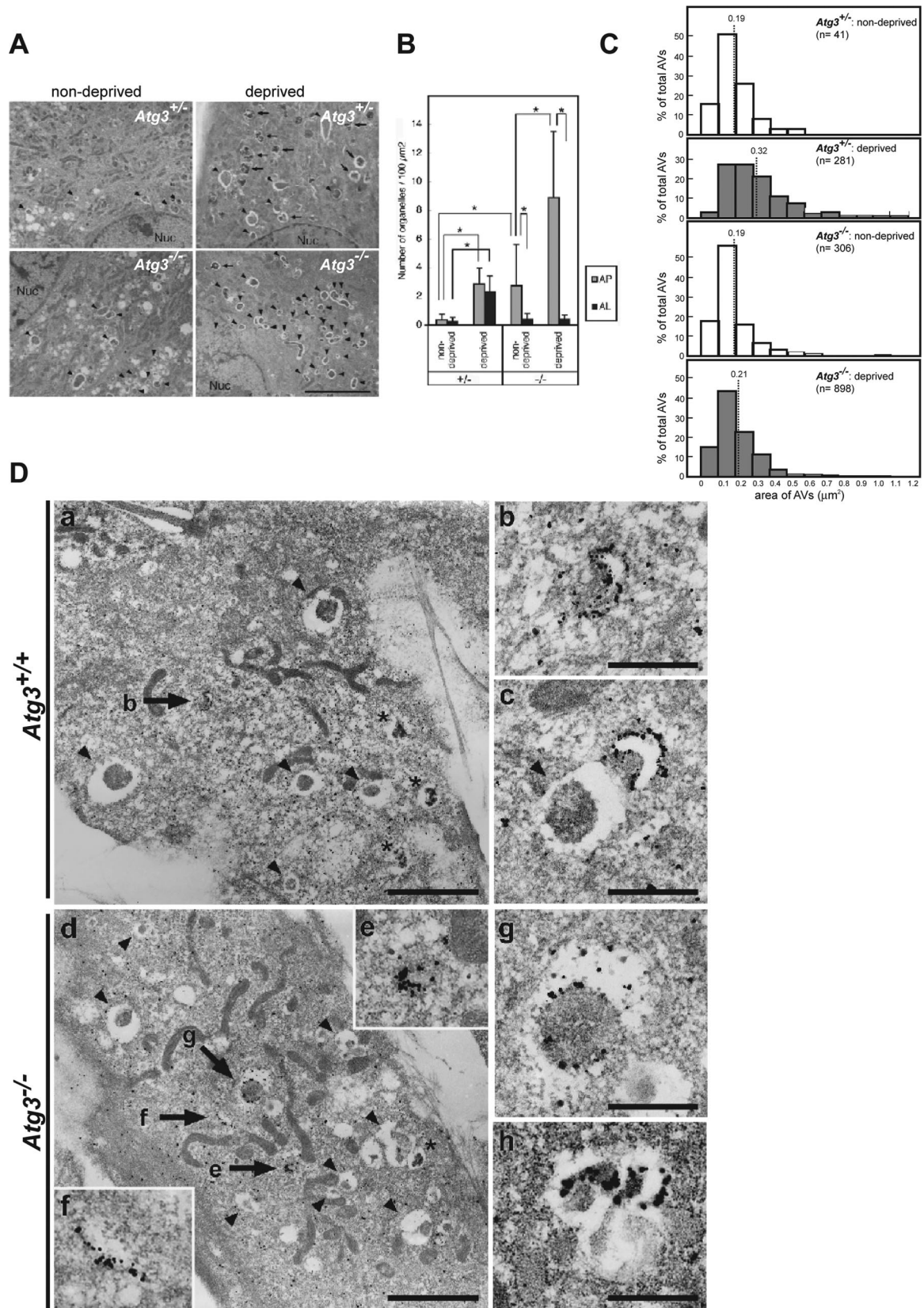
Figure 5. Induction of autophagosomes under starvation condition in *Atg3*-knockout cells. (A) Electron micrographs of primary MEFs from the indicated genotype mice under nutrient-rich (nondeprived) or -poor (deprived) condition. Bar, 5 μm. Arrowheads, autophagosomes; arrows, autolysosomes. (B) Numbers of autophagosomes (AP) and autolysosomes (AL) in each genotype were counted (n = 20; for details, see *Materials and Methods*). Data are mean ± SD. *p < 0.01, by Student's *t* test. (C) Area of autophagosome-like vacuoles (AVs) in MEFs from the indicated genotype under nutrient-rich (nondeprived) and -poor (deprived) conditions. Frequencies (percentages) of the given range of

der poor nutrient condition. In wild-type MEFs, nutrient deprivation induced a significant protein degradation, which was suppressed by the addition of lysosomal inhibitors, 3-methyladenine (3-MA), E64d, pepstatin, and ammonium chloride (E64d/PepA + AC) (Figure 6A). The induced degradation was also inhibited by treatment with lactacystin, a proteasome inhibitor, although the inhibition was less than that observed with lysosomal inhibitors (Figure 6A). These results suggest that starvation-induced protein degradation is mainly mediated through the lysosomal pathway in MEFs. Although degradation of long-lived protein was induced by nutrient deprivation even in $Atg3^{-/-}$ MEFs, the level was significantly lower than in wild-type MEFs (Figure 6A) and comparable with that in $Atg7$-deficient MEFs (Figure 6B). However, it is likely that other pathways such as chaperone-mediated autophagy and microautophagy also mediate starvation-induced protein degradation in $Atg3$- and $Atg7$-deficient MEFs, although to a lesser extent, consistent with recent reports (Kiffin et al., 2006; Massey et al., 2006). Together, we concluded that nutrient-deprivation induced the formation of small autophagosome-like structures but not autolysosomes in $Atg3$-knockout cells.

Impairment of Closing Step of Autophagosome Formation Followed by Appearance of Aberrant Membranous Structures in Atg3-deficient MEFs

We further examined in more details the autophagosome-like structures in serial sections. A conventional autophagosome in wild-type MEF consists of a single mass of engulfed material surrounded by a single isolation membrane, and the whole structure looked round or elliptical (Figure 7, A–D), as has been described extensively. We also found that more than half of the autophagosomes were not closed and the engulfed contents were continuous with the cytoplasm. In $Atg3$-deficient MEF, however, the engulfed portion was often divided by an isolation membrane that seemed to elongate in a random manner (Figure 7, F and H). Therefore, in some cases, the single set of autophagosome-like structures looked like a cluster of small autophagosomes, whereas in others, they looked just like an abnormally elongated structure (Figure 5A). The frequency of such aberrant structures in $Atg3$-deficient MEFs (22.0 ± 10.2% of AVi) was significantly (p < 0.01 by Student's t test) higher than those in wild-type MEFs (5.5 ± 5.9% of AVi). We could not compare the proportion of unclosed autophagosome-like structures between wild-type and $Atg3$-deficient MEFs because of the complex membranous extensions in the mutant MEFs and the limitation of using serial sections, in which we can observe objects along only a given direction. Nevertheless, these results strongly suggest that Atg8 system is indispensable for the proper elongation step of isolation membranes, and probably their closure.

Figure 5 (cont). area are expressed in the histogram. The dotted line represents the mean value of the area in each genotype. (D) Immunoelectron micrograph showing labeling of GFP (a and b) and Atg16L (c–h) in wild-type (a–c) and $Atg3$-deficient MEFs (d–h) harboring GFPAtg5 under nutrient deprivation conditions. b is a higher magnification view of the GFPAtg5-positive structure indicated by the arrow in a. Higher magnification views of the Atg16L-positive structures indicated by arrows in d are shown in insets e and f. Arrowheads indicate autophagosome-like structures without GFPAtg5 or Atg16L signal. Asterisks indicate autolysosomes. Bars, 0.5 μm.
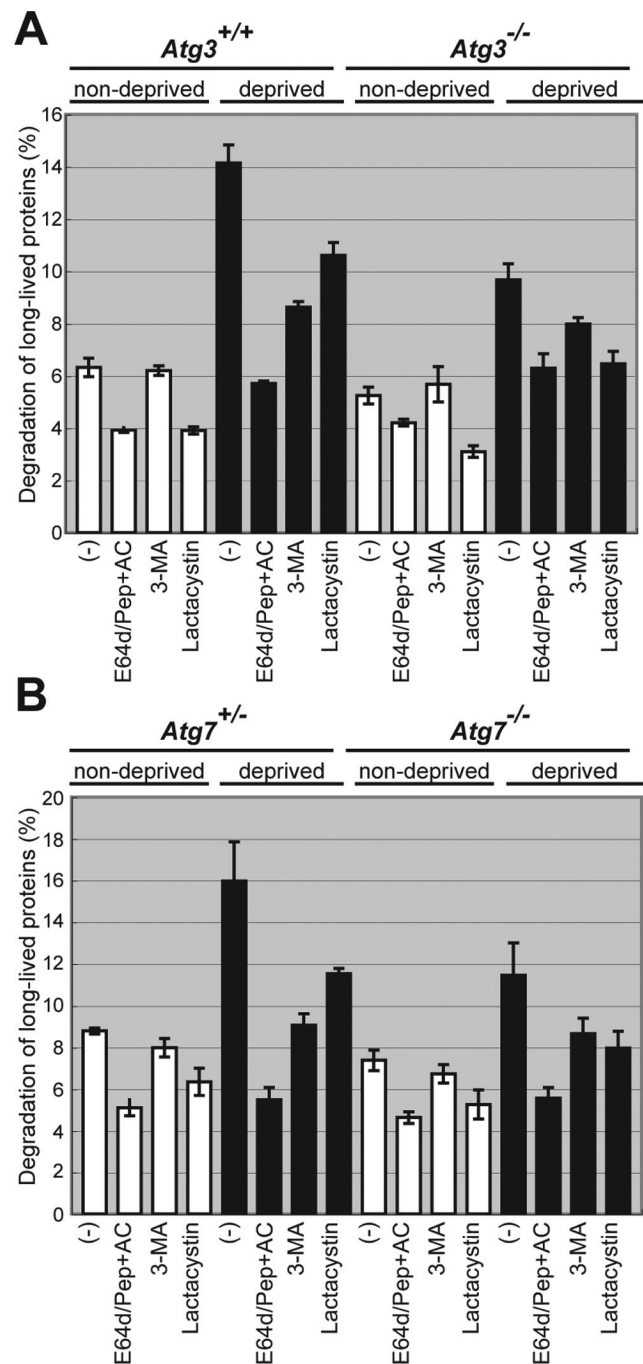
Figure 6. (A and B) Impaired long-lived protein degradation in $Atg3$-deficient MEFs. Primary MEFs from wild-type, $Atg3$- (A) and $Atg7$-knockout (B) mice were isolated and labeled with [^{14}C]leucine for 24 h, and degradation of long-lived protein in deprived and nondeprived conditions was measured. 3-MA and/or E64d, pepstatin A and ammonium chloride (E64d/Pep + AC), or lactacystin was added as indicated. Data are mean ± SD of triplicate experiments.

Suppression of Development of Early Isolation Membranes and Appearance of Aberrant Membranous Structures in Atg3-deficient Hepatocytes

Finally, to investigate whether the autophagosome-like structures are found in other $Atg3$-deficient mouse tissues, we examined the liver of heterozygous and $Atg3$-knockout
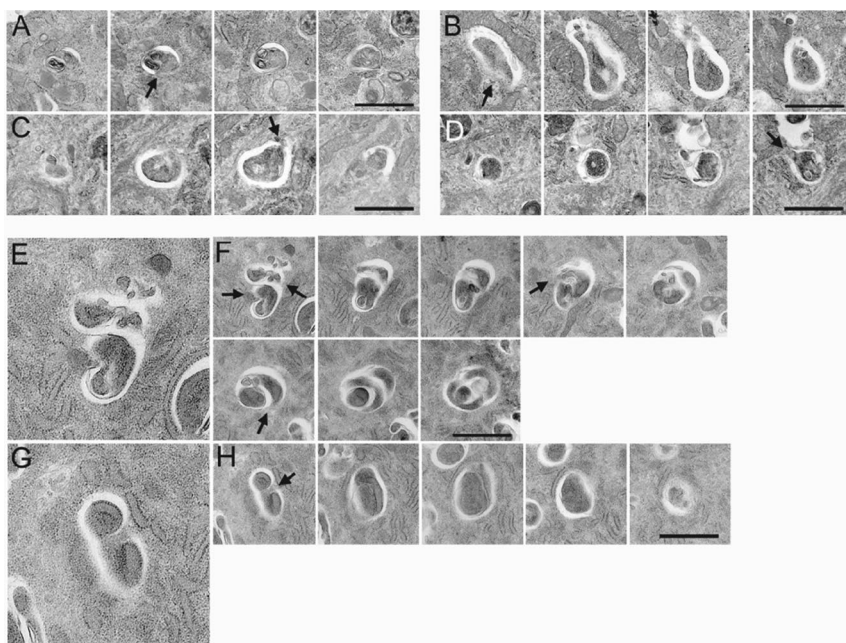
Y.-S. Sou *et al.*

Figure 7. Impaired elongation and closure in autophagosome formation in *Atg3*-deficient MEFs. Electron microscopic analyses of serial sections of wild-type (A–D) and *Atg3*-deficient MEFs (E–H). Arrows indicate open regions of autophagosome-like structures. Note that the isolation membranes seem to elongate in random directions, thus these membranes sequestrate certain area of the cytoplasm in some parts. Therefore, isolation membranes in mutant cells did not close to form complete autophagosomes. Bars, 1 μm.

neonates under starvation condition after Caesarean delivery. Immunofluorescence microscopy using anti-Atg16L antibody showed that numerous Atg16L-positive structures occurred in heterozygous liver, but such structures were hardly observed in the mutant liver (Figure 8A). Instead, some pleomorphic structures weakly positive for Atg16L were often observed in *Atg3*-deficient hepatocytes (Figure 8A, arrow). Subsequent electron microscopic analyses revealed a tendency for a smaller glycogen area in mutant hepatocytes than heterozygous hepatocytes (Figure 8B, a and b), similar to *Atg7*-deficient adult hepatocytes (Komatsu *et al.*, 2005). Although the nutrient-deprived heterozygous hepatocytes contained typical autophagosomes (Figure 8Bc), the number of such structures was significantly lower in nutrient-deprived mutant hepatocytes (Figure 8Bb). Instead, the *Atg3*-knockout hepatocytes occasionally contained aberrant membranous complexes that sometimes resembled the autophagosomes. However, the membranes were often elongated and wrapped more than two cytoplasmic portions and/or wrapped a portion several times, forming a multilamellar structure. These results strengthen the hypothesis that the Atg8 system is indispensable for the regulated elongation of isolation membranes, and its defect leads to the formation of autophagosome-like structures, such as multilamellar structures.

DISCUSSION

In this study, we showed the roles of Atg3, a specific E2-like enzyme for Atg8, in the autophagic pathway by generating *Atg3* null-mice. Although *Atg3*-deficient mice displayed no apparent developmental defects based on our histological analyses (Supplemental Figure S5), they died within 1 d after birth, similar to *Atg5*- and *Atg7*-deficient mice (Kuma *et al.*, 2004; Komatsu *et al.*, 2005). The short survival time after Caesarean delivery of *Atg3*-deficient mice was comparable with those of other autophagy-deficient mice such as *Atg5* and *Atg7* mice (Kuma *et al.*, 2004; Komatsu *et al.*, 2005). Furthermore, the low concentration of amino acids in *Atg3*-deficient mice after starvation was similar to those in *Atg5*-

and *Atg7*-deficient mice (Figure 2) (Kuma *et al.*, 2004; Komatsu *et al.*, 2005). We reported recently that autophagy is responsible for constitutive protein turnover in quiescent hepatocytes and neurons even under nutrient-rich conditions and that defects in autophagy lead to accumulation of ubiquitin-containing large inclusions (Komatsu *et al.*, 2005; 2006; Hara *et al.*, 2006). Thus, we expected that ubiquitin-positive inclusions would also be present in *Atg3*-deficient mice. Such inclusions were observed in the pons and hepatocytes of *Atg3*-deficient mice at P0 (data not shown). All examined phenotypes of *Atg3*-knockout mice resembled those of other *Atg* knockout mice. All results are consistent with impaired autophagy in *Atg3*-deficient cells.

Our results showed that *Atg3* is essential for Atg8-conjugation in mammals (Figure 1). Immunofluorescent analyses revealed that LC3 did not form cup-shaped or ring-like structure in *Atg3*-deficient MEFs and myocardium (Figures 1 and 2). In mammals, LC3 has at least two other homologues, GABARAP and GATE-16, which share common biochemical characteristics and localize to autophagosomes (Tanida *et al.*, 2001, 2002; Kabeya *et al.*, 2004). The modification and levels of these molecules were also affected in the mutant MEFs. Similar to LC3 states, mutant cells showed impairment of modification of GABARAP, whereas the PE-conjugated form was observed in the wild-type cells under both nutrient-rich and -deprived conditions. Because the modified forms of LC3 and GABARAP were formed even in nutrient-rich conditions, they might play a role in constitutive autophagy, which occurs irrelevant of the nutrient state, in addition to their roles in starvation-induced autophagy. Although neither GATE-16-I nor GATE-16-II was detected in wild-type cells under both nutrient-available and -deprived conditions, GATE-16-I was clearly detected in mutant cells, suggesting that GATE-16 might be rapidly degraded depending on the autophagic pathway. Actually, treatment with lysosomal inhibitor led to acute accumulation of GATE-16-II (Supplemental Figure S1). These findings are similar to those observed in *Atg7*-deficient mice (Komatsu *et al.*, 2005). The difference of action among Atg8 homologues in their response to nutrient conditions might
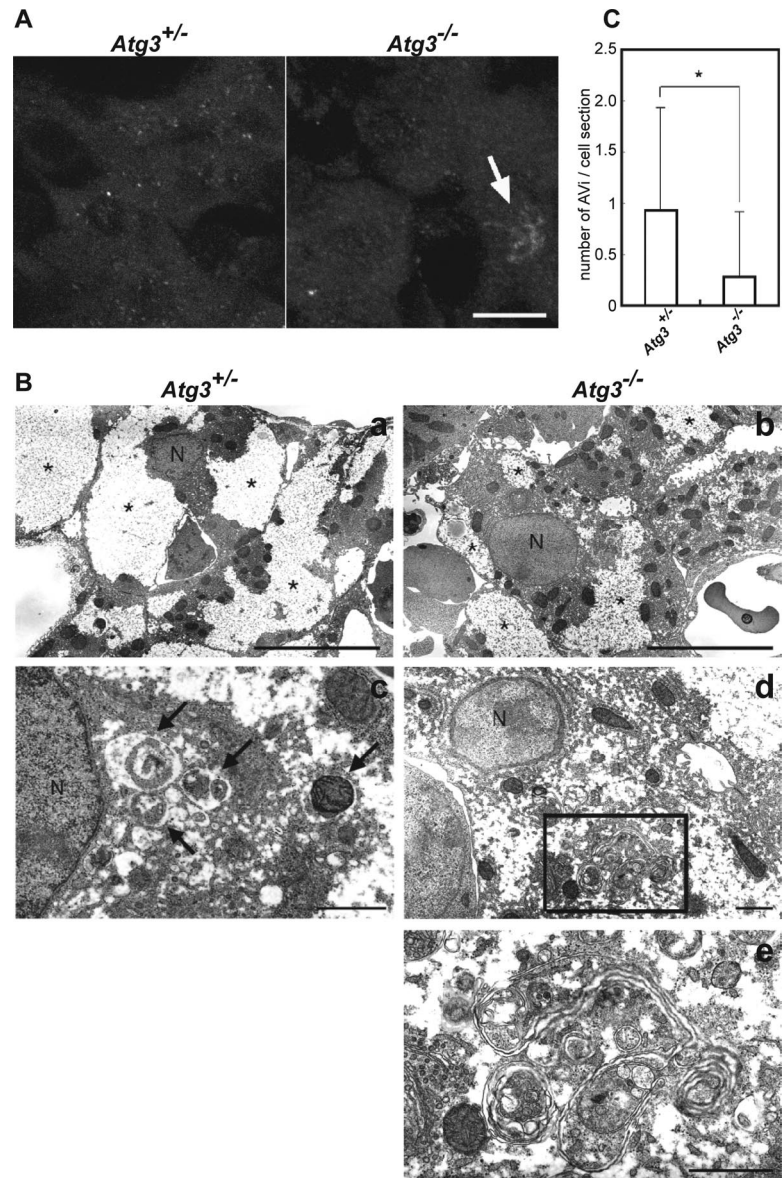

Molecular Biology of the Cell

Figure 8. Suppression of formation of early isolation membranes and appearance of aberrant membranous structures in *Atg3*-deficient hepatocytes. (A) Immunofluorescence analysis of Atg16L in hepatocytes from *Atg3*$^{+/-}$ (left) and *Atg3*$^{-/-}$ (right) newborn mice. Each newborn mouse was fixed at 6 h after Cesarean delivery. Atg16L-positive structures were observed in *Atg3*$^{+/-}$, but only few in *Atg3*$^{-/-}$ neonate hepatocytes. Arrow indicates a pleomorphic structure positive for Atg16L. Bar, 10 μm. (B) Electron microscopic analysis of hepatocytes from *Atg3*$^{+/-}$ (a and c) and *Atg3*$^{-/-}$ (b, d, and e) newborn mice. Each newborn mouse was fixed for electron microscopy at 6 h after Cesarean delivery. Typical autophagosomes (arrows) were observed in *Atg3*$^{+/-}$, but fewer in *Atg3*$^{-/-}$ neonatal hepatocytes. Aberrant membranous structures occurred in *Atg3*$^{-/-}$ neonate hepatocytes (d and e). e is a magnification view of the boxed region in d. Note that the glycogen area (asterisks) is smaller in mutant hepatocytes than heterozygous hepatocytes. N, nucleus. Bars, 10 μm (a and b) and 1 μm (c–e). (C) The number of autophagosomes in a section of hepatocyte in each genotype (mean ± SD; n = 60). *p < 0.001.

reflect their distinct roles in constitutive or starvation-induced autophagy. We sought to determine their localizations under nutrient-rich and deprived conditions, but our antibodies for these molecules were not applicable for immunofluorescent analyses. Further analysis is required to unravel the roles of GABARAP and GATE-16 in autophagy, and such analysis is currently underway by generating transgenic mice harboring each GFP-GABARAP and GFP-GATE-16 (Tanida and Kominami, unpublished data).

Intriguingly, *Atg5* deficiency affects another line of conjugation system that causes significant reduction in the conversion of LC3 to PE-conjugated form in yeast and mice (Mizushima *et al.*, 2001; Suzuki *et al.*, 2001; Hosokawa *et al.*, 2007). Moreover, Atg10, a specific E2 enzyme for Atg12, interacts with LC3, and overproduction of Atg10 accelerates conversion into the LC3-II form (Nemoto *et al.*, 2003). Furthermore, overproduction of Atg3 promotes the formation of Atg12–Atg5 conjugates (Tanida *et al.*, 2002). These results strongly suggest functional cooperation between the two conjugation systems. However, the role of Atg8 system in Atg12 system based on the loss of function has not yet been

examined so far. In this study, we showed that *Atg3* deficiency markedly inhibits the formation of the Atg12–Atg5 conjugate (Figure 3). Why is Atg12–Atg5 conjugation suppressed by loss of Atg3? Comprehensive analyses of yeast two-hybrid screening revealed interaction between Atg3 and Atg12 in yeast (Uetz *et al.*, 2000). This physical interaction was also confirmed in mammalian cells (Tanida *et al.*, 2002). This interaction might be critical for effective formation of the Atg12–Atg5 conjugate. However, in in vitro reconstitution assay for the Atg12–Atg5 conjugate in the presence or absence of Atg3 protein, we could not detect enhanced formation of the Atg12–Atg5 conjugate (Supplemental Figure S6), suggesting the involvement of other cellular factor(s) in the accelerated formation of the Atg12–Atg5 conjugate by Atg3. Indeed, unlike the in vitro results, inhibition of Atg12–Atg5 conjugate formation was complemented by exogenous expression of wild-type but not the active site mutant of Atg3 into *Atg3*-deficient MEFs (Figure 3), implying that the Atg8/LC3-conjugation system might assist Atg12–Atg5 conjugation reaction. Another possibility is that the retarded dissociation of Atg12–Atg5 conjugate

from the isolation membrane (Figures 4 and 5) might suppress any new conjugation between Atg12 and Atg5. Further analysis is required to unravel the role of Atg3 in the formation of the Atg12–Atg5 conjugate.

Although both Atg8 and its homologue LC3 are considered suitable markers for autophagosomes (Kabeya *et al.*, 2000; Kirisako *et al.*, 2000; Mizushima *et al.*, 2004), their functions in autophagosome formation are poorly understood. Herein, we showed that loss of *Atg3* was associated with autophagosome malformation with defects in multiple steps of autophagosome formation after generation of early isolation membranes. The first defect was failure of localization of LC3 to the isolation membranes due to the loss of its conjugation to PE (Figure 1). Second, the absence of LC3 on the isolation membrane led to delay of dissociation of Atg12–Atg5–Atg16L complex from the membrane (Figure 4). Third, the loss of LC3-PE and/or prolonged association of Ag12–Atg5–Atg16L complex with the membranes caused a dysregulated elongation of isolation membranes in response to nutrient deprivation (Figure 5). Fourth, loss of LC3-PE on the isolation membranes caused impairment of fusion of each membrane sac, resulting in the accumulation of unclosed autophagosome-like structures, some of which could be seen as multilamellar structures in hepatocytes (Figures 7 and 8). The fourth criterion is in agreement with the data showing accumulation of intermediate autophagic structures (isolation membranes) in cells with almost complete impairment of LC3 conjugation by overexpression of Atg4B (Fujita, Noda, and Yoshimori, personal communication). These findings emphasize the indispensable role of the Atg8/LC3 system in the development of isolation membranes, consistent with a recent report in yeasts (Nakatogawa *et al.*, 2007), although we could not exclude the involvement of Atg8 system in the fusion of autophagosomes with lysosomes.

Although numerous early isolation membranes double-positive for Atg16L- and Atg5 were observed in *Atg3*-deficient MEFs, we think that incidence of these isolation membranes in *Atg3*-deficient mice are probably lower than that in wild-type mice. Because the half-life of autophagosomes is ~10 min (Mizushima *et al.*, 2001), if the isolation membranes in mutant mice were normally developed and only their elongation and closing steps were impaired, numerous autophagosome-like structures should accumulate in mutant mice. However, their number after 2-h starvation in the mutant remained twofold that in wild-type MEFs (Figure 5), suggesting a low production of the isolation membranes in *Atg3* deficiency. This conclusion is also supported by the reduced production of Atg16L-positive structures in *Atg3*-deficient hepatocytes (Figure 8). Moreover, time-lapse analysis revealed fewer de novo GFPAtg5 dots in mutant MEFs. Therefore, we infer that *Atg3* deficiency affects the generation of early isolation membranes, as well as their development. We stress that almost all phenotypes observed in *Atg3*-deficient mice were due to impaired Atg8-system rather than low production of Atg12–Atg5 conjugate because the presence of a very low level of Atg12–Atg5 is sufficient for autophagy (Hosokawa *et al.*, 2007).

Importantly, small autophagosome-like structures observed in *Atg3*-deficient MEFs were also recognized in *Atg7*-deficient MEFs (our unpublished data). In addition, several elongated isolation membranes and numerous double membrane structures were found even in *Atg5*-deficient ES cells and Purkinje cells, respectively (Mizushima *et al.*, 2001; Nishiyama *et al.*, 2007). Moreover, membrane complex structures recognized in *Atg3*-deficient neonate hepatocytes resemble the multilamellar structures observed in *Atg7*-defi-

cient adult hepatocytes (Komatsu *et al.*, 2005). Furthermore, such multilamellar structures were also observed in *Atg5*- and *Atg7*-deficient Purkinje cells (Komatsu *et al.*, 2007; Nishiyama *et al.*, 2007). Therefore, the Atg8 system and perhaps the Atg12 system may be essential for proper membrane development and closure for the completion of autophagosome formation. Our *Atg3* mutant mice, together with *Atg5*$^{-/-}$ and *Atg7*$^{-/-}$ mice, should be useful for examining and delineating autophagosome formation in mammalian cells.

REFERENCES

Cuervo, A. M. (2004). Autophagy: in sickness and in health. Trends Cell Biol. *14*, 70–77.

Fujita, N., Itoh, T., Omori, H., Fukuda, M., Noda, T., and Yoshimori, T. (2008). The Atg16L complex specifies the site of LC3 lipidation for membrane biogenesis in autophagy. Mol. Biol. Cell *19*, 2092–2100.

Goldberg, A. L. (2003). Protein degradation and protection against misfolded or damaged proteins. Nature *426*, 895–899.

Gutierrez, M. G., Master, S. S., Singh, S. B., Taylor, G. A., Colombo, M. I., and Deretic, V. (2004). Autophagy is a defense mechanism inhibiting BCG and *Mycobacterium tuberculosis* survival in infected macrophages. Cell *119*, 753–766.

Hanada, T., Noda, N. N., Satomi, Y., Ichimura, Y., Fujioka, Y., Takao, T., Inagaki, F., and Ohsumi, Y. (2007). The Atg12-Atg5 conjugate has a novel E3-like activity for protein lipidation in autophagy. J. Biol. Chem. *282*, 37298–37302.

Hanaoka, H., Noda, T., Shirano, Y., Kato, T., Hayashi, H., Shibata, D., Tabata, S., and Ohsumi, Y. (2002). Leaf senescence and starvation-induced chlorosis are accelerated by the disruption of an *Arabidopsis* autophagy gene. Plant Physiol. *129*, 1181–1193.

Hara, T. *et al*. (2006). Suppression of basal autophagy in neural cells causes neurodegenerative disease in mice. Nature *441*, 885–889.

Hosokawa, N., Hara, Y., and Mizushima, N. (2007). Generation of cell lines with tetracycline-regulated autophagy and a role for autophagy in controlling cell size. FEBS Lett. *581*, 2623–2629.

Ichimura, Y. *et al*. (2000). A ubiquitin-like system mediates protein lipidation. Nature *408*, 488–492.

Ichimura, Y., Kumanomido, T., Sou, Y. S., Mizushima, T., Ezaki, J., Ueno, T., Kominami, E., Yamane, T., Tanaka, K., and Komatsu, M. (2008). Structural basis for sorting mechanism of p62 in selective autophagy. J. Biol. Chem. *283*, 22847–22857.

Kabeya, Y., Mizushima, N., Ueno, T., Yamamoto, A., Kirisako, T., Noda, T., Kominami, E., Ohsumi, Y., and Yoshimori, T. (2000). LC3, a mammalian homologue of yeast Apg8p, is localized in autophagosome membranes after processing. EMBO J. *19*, 5720–5728.

Kabeya, Y., Mizushima, N., Yamamoto, A., Oshitani-Okamoto, S., Ohsumi, Y., and Yoshimori, T. (2004). LC3, GABARAP and GATE16 localize to autophagosomal membrane depending on form-II formation. J. Cell Sci. *117*, 2805–2812.

Kiffin, R., Bandyopadhyay, U., and Cuervo, A. M. (2006). Oxidative stress and autophagy. Antioxid. Redox Signal. *8*, 152–162.

Kirisako, T., Ichimura, Y., Okada, H., Kabeya, Y., Mizushima, N., Yoshimori, T., Ohsumi, M., Takao, T., Noda, T., and Ohsumi, Y. (2000). The reversible modification regulates the membrane-binding state of Apg8/Aut7 essential for autophagy and the cytoplasm to vacuole targeting pathway. J. Cell Biol. *151*, 263–276.

Kitamura, T., Koshino, Y., Shibata, F., Oki, T., Nakajima, H., Nosaka, T., and Kumagai, H. (2003). Retrovirus-mediated gene transfer and expression cloning: powerful tools in functional genomics. Exp. Hematol. *31*, 1007–1014.

Klionsky, D. J. (2005). The molecular machinery of autophagy: unanswered questions. J. Cell Sci. *118*, 7–18.

Komatsu, M. *et al*. (2005). Impairment of starvation-induced and constitutive autophagy in Atg7-deficient mice. J. Cell Biol. *169*, 425–434.

Komatsu, M. *et al*. (2006). Loss of autophagy in the central nervous system causes neurodegeneration in mice. Nature *441*, 880–884.

Komatsu, M., Wang, Q. J., Holstein, G. R., Friedrich, V. L., Jr., Iwata, J., Kominami, E., Chait, B. T., Tanaka, K., and Yue, Z. (2007). Essential role for autophagy protein Atg7 in the maintenance of axonal homeostasis and the prevention of axonal degeneration. Proc. Natl. Acad. Sci. USA *104*, 14489–14494.

Kuma, A., Hatano, M., Matsui, M., Yamamoto, A., Nakaya, H., Yoshimori, T., Ohsumi, Y., Tokuhisa, T., and Mizushima, N. (2004). The role of autophagy during the early neonatal starvation period. Nature *432*, 1032–1036.

Kuma, A., Mizushima, N., Ishihara, N., and Ohsumi, Y. (2002). Formation of the approximately 350-kDa Apg12-Apg5.Apg16 multimeric complex, mediated by Apg16 oligomerization, is essential for autophagy in yeast. J. Biol. Chem. *277*, 18619–18625.

Lee, G. H., Ogawa, K., and Drinkwater, N. R. (1995). Conditional transformation of mouse liver epithelial cells. An in vitro model for analysis of genetic events in hepatocarcinogenesis. Am. J. Pathol. *147*, 1811–1822.

Levine, B., and Klionsky, D. J. (2004). Development by self-digestion: molecular mechanisms and biological functions of autophagy. Dev. Cell *6*, 463–477.

Massey, A. C., Kaushik, S., Sovak, G., Kiffin, R., and Cuervo, A. M. (2006). Consequences of the selective blockage of chaperone-mediated autophagy. Proc. Natl. Acad. Sci. USA *103*, 5805–5810.

Mizushima, N., Kuma, A., Kobayashi, Y., Yamamoto, A., Matsubae, M., Takao, T., Natsume, T., Ohsumi, Y., and Yoshimori, T. (2003). Mouse Apg16L, a novel WD-repeat protein, targets to the autophagic isolation membrane with the Apg12-Apg5 conjugate. J. Cell Sci. *116*, 1679–1688.

Mizushima, N., Noda, T., Yoshimori, T., Tanaka, Y., Ishii, T., George, M. D., Klionsky, D. J., Ohsumi, M., and Ohsumi, Y. (1998a). A protein conjugation system essential for autophagy. Nature *395*, 395–398.

Mizushima, N., Ohsumi, Y., and Yoshimori, T. (2002). Autophagosome formation in mammalian cells. Cell Struct. Funct. *27*, 421–429.

Mizushima, N., Sugita, H., Yoshimori, T., and Ohsumi, Y. (1998b). A new protein conjugation system in human. The counterpart of the yeast Apg12p conjugation system essential for autophagy. J. Biol. Chem. *273*, 33889–33892.

Mizushima, N., Yamamoto, A., Hatano, M., Kobayashi, Y., Kabeya, Y., Suzuki, K., Tokuhisa, T., Ohsumi, Y., and Yoshimori, T. (2001). Dissection of autophagosome formation using Apg5-deficient mouse embryonic stem cells. J. Cell Biol. *152*, 657–668.

Mizushima, N., Yamamoto, A., Matsui, M., Yoshimori, T., and Ohsumi, Y. (2004). In vivo analysis of autophagy in response to nutrient starvation using transgenic mice expressing a fluorescent autophagosome marker. Mol. Biol. Cell *15*, 1101–1111.

Nakagawa, I. *et al*. (2004). Autophagy defends cells against invading group A Streptococcus. Science *306*, 1037–1040.

Nakatogawa, H., Ichimura, Y., and Ohsumi, Y. (2007). Atg8, a ubiquitin-like protein required for autophagosome formation, mediates membrane tethering and hemifusion. Cell *130*, 165–178.

Nemoto, T., Tanida, I., Tanida-Miyake, E., Minematsu-Ikeguchi, N., Yokota, M., Ohsumi, M., Ueno, T., and Kominami, E. (2003). The mouse APG10 homologue, an E2-like enzyme for Apg12p conjugation, facilitates MAP-LC3 modification. J. Biol. Chem. *278*, 39517–39526.

Nishiyama, J., Miura, E., Mizushima, N., Watanabe, M., and Yuzaki, M. (2007). Aberrant membranes and double-membrane structures accumulate in the axons of Atg5-null Purkinje cells before neuronal death. Autophagy *3*, 591–596.

Ohsumi, Y. (2001). Molecular dissection of autophagy: two ubiquitin-like systems. Nat. Rev. Mol. Cell Biol. *2*, 211–216.

Shintani, T., Mizushima, N., Ogawa, Y., Matsuura, A., Noda, T., and Ohsumi, Y. (1999). Apg10p, a novel protein-conjugating enzyme essential for autophagy in yeast. EMBO J. *18*, 5234–5241.

Sou, Y. S., Tanida, I., Komatsu, M., Ueno, T., and Kominami, E. (2006). Phosphatidylserine in addition to phosphatidylethanolamine is an in vitro target of the mammalian Atg8 modifiers, LC3, GABARAP, and GATE-16. J. Biol. Chem. *281*, 3017–3024.

Suzuki, K., Kirisako, T., Kamada, Y., Mizushima, N., Noda, T., and Ohsumi, Y. (2001). The pre-autophagosomal structure organized by concerted functions of APG genes is essential for autophagosome formation. EMBO J. *20*, 5971–5981.

Tanida, I., Mizushima, N., Kiyooka, M., Ohsumi, M., Ueno, T., Ohsumi, Y., and Kominami, E. (1999). Apg7p/Cvt2p: a novel protein-activating enzyme essential for autophagy. Mol. Biol. Cell *10*, 1367–1379.

Tanida, I., Sou, Y. S., Ezaki, J., Minematsu-Ikeguchi, N., Ueno, T., and Kominami, E. (2004). HsAtg4B/HsApg4B/autophagin-1 cleaves the carboxyl termini of three human Atg8 homologues and delipidates microtubule-associated protein light chain 3- and GABAA receptor-associated protein-phospholipid conjugates. J. Biol. Chem. *279*, 36268–36276.

Tanida, I., Tanida-Miyake, E., Komatsu, M., Ueno, T., and Kominami, E. (2002). Human Apg3p/Aut1p homologue is an authentic E2 enzyme for multiple substrates, GATE-16, GABARAP, and MAP-LC3, and facilitates the conjugation of hApg12p to hApg5p. J. Biol. Chem. *277*, 13739–13744.

Tanida, I., Tanida-Miyake, E., Ueno, T., and Kominami, E. (2001). The human homolog of *Saccharomyces cerevisiae* Apg7p is a protein-activating enzyme for multiple substrates including human Apg12p, GATE-16, GABARAP, and MAP-LC3. J. Biol. Chem. *276*, 1701–1706.

Thumm, M., Egner, R., Koch, B., Schlumpberger, M., Straub, M., Veenhuis, M., and Wolf, D. H. (1994). Isolation of autophagocytosis mutants of *Saccharomyces cerevisiae*. FEBS Lett. *349*, 275–280.

Tsukada, M., and Ohsumi, Y. (1993). Isolation and characterization of autophagy-defective mutants of *Saccharomyces cerevisiae*. FEBS Lett. *333*, 169–174.

Uetz, P. *et al*. (2000). A comprehensive analysis of protein-protein interactions in. *Saccharomyces cerevisiae*. Nature *403*, 623–627.